

A new and efficient implementation of CC3

Alexander C. Paul,[†] Rolf H. Myhre,[†] and Henrik Koch^{*,†,‡}

[†]*Department of Chemistry, Norwegian University of Science and Technology, NTNU, 7491
Trondheim, Norway*

[‡]*Scuola Normale Superiore, Piazza dei Cavalieri 7, 56126 Pisa, Italy*

E-mail: henrik.koch@sns.it

Abstract

We present a new and efficient implementation of the closed shell coupled cluster singles and doubles with perturbative triples method (CC3) in the electronic structure program e^T . Asymptotically, a ground state calculation scales as $2n_V^4 n_O^3$ where n_V and n_O are the number of virtual and occupied orbitals respectively. The Jacobian and transpose Jacobian transformations, required to compute excitation energies and transition moments, both scale iteratively as $4n_V^4 n_O^3$. We have also implemented equation-of-motion (EOM) transition moments for CC3. The EOM transition densities require recalculation of triples amplitudes, as N^6 tensors are not stored in memory. This results in a noniterative computational cost of $5n_V^4 n_O^3$ for the ground state density and $13n_V^4 n_O^3$ per state for the transition densities. We demonstrate the computational efficiency of the implementation by calculating valence and core excited states of L-proline.

Introduction

Highly brilliant X-ray sources like synchrotrons and X-ray free electron lasers are increasingly becoming routine for the spectroscopic community. X-ray spectroscopies such as near edge

X-ray absorption fine structure (NEXAFS) can provide a detailed insight into the electronic structure of molecules and their environment.^{1,2} Accurate modelling makes it possible to interpret the spectroscopic data generated by these techniques, providing new insights into the underlying chemistry.

High energy excitations, such as those measured in X-ray spectroscopy are challenging to model because they typically generate a core hole. This, in turn, results in a large contraction of the electron density that requires high level models to describe.³ In order to describe these relaxation effects accurately, triple excitations must be included in the wave function description.^{4,5}

Coupled cluster theory is the preferred model for calculating spectroscopic properties for molecules, combining high accuracy and correct scaling with system size in the coupled cluster response theory (CCRT) formulation.⁶⁻⁸ Coupled cluster singles and doubles (CCSD) is the most widely used variant of coupled cluster, due to its high accuracy and relatively feasible computational scaling of N^6 with system size. Nevertheless, for some properties like core excitation energies, CCSD can deviate by several electron volts from experimental values. These deviations are reduced by an order of magnitude if triples are included in the description of the wave function.^{4,9} However, coupled cluster singles, doubles and triples (CCSDT) is unfeasible due to the N^6 memory requirement and N^8 computational cost. Approximating the triples amplitudes can reduce the scaling to N^7 and the memory requirement to N^4 .

These approximate models are typically categorized as noniterative and iterative models. For the noniterative models, a triples energy correction is computed after solving the CCSD equations. The terms included in the energy correction are usually determined based on a many-body perturbation theory (MBPT) like expansion of the energy.¹⁰⁻¹³ However, by far the most popular of these methods, CCSD(T), does not follow a strict MBPT expansion of the energy. For CCSD(T) the energy is expanded consistently to fourth order and one additional fifth order term is added for no apparent reason.¹⁴ It was later shown that CCSD(T) can be viewed as an MBPT like expansion from the CCSD wave function.¹⁵ A

related method is the ACCSD(T) method where the parameters of the left wave function are included in the MBPT expansion.¹⁶ While the noniterative methods are much cheaper computationally than the iterative methods, most of them are only suited for ground state calculations. An exception is the CCSD(T)(a) model that also includes triples corrections to the excitation energies.¹⁷ The iterative models are more expensive, but they can also be more accurate. The CCSDT-n models¹⁸ and CC3^{19,20} are the most well known of these methods. The two models have the same computational cost, but CC3 is more accurate due to the full inclusion of single excitation amplitudes.²¹ For a more extensive discussion of approximate triples methods, see Ref. 22.

Due to the high computational cost, an efficient CC3 implementation is required for larger molecules.^{19,20} In this paper we present an implementation of CC3 ground and excited states, as well as equation-of-motion (EOM)²³ transition moments. Although the EOM formalism has been shown to be less accurate than CCRT for transition moments,⁷ the differences are believed to be small for high level methods like CC3.²⁴ The current implementation scales iteratively as $2n_V^4 n_O^3$ for the ground state and $4n_V^4 n_O^3$ for excited states, where n_V is the number of virtual and n_O is the number of occupied orbitals. Note that this is less than the minimum of $5n_V^4 n_O^3$ stated in the literature.²⁵ For core excited states, we use the core valence separation (CVS) approximation.²⁶⁻²⁸ This reduces the iterative computational cost to $4n_V^4 n_O^2$ for excitation energies, however, the scaling of the ground state calculation remains unchanged.

Theory

In this section, we will derive the equations for CC3 within the EOM formalism. Consider the coupled cluster wave function,

$$|\text{CC}\rangle = e^T |\text{R}\rangle \quad T = \sum_{\mu} \tau_{\mu} X_{\mu}. \quad (1)$$

Here, $|\mathbf{R}\rangle$ is a reference Slater determinant, usually the Hartree-Fock wave function, and T is the cluster operator with μ labeling excited determinants. The excitation operator, X_μ , maps the reference, $|\mathbf{R}\rangle$ into determinant $|\mu\rangle$ and τ_μ is the corresponding parameter, referred to as an amplitude.

In order to obtain the ground state energy, we introduce a biorthonormal parametrization for the left vector,

$$\langle\tilde{\mathbf{C}}\mathbf{C}| = \langle\mathbf{R}|(1 + \Lambda)e^{-T} \quad \Lambda = \sum_{\mu \neq \mathbf{R}} \lambda_\mu X_\mu^\dagger. \quad (2)$$

Inserting these expressions into the Schrödinger equation, we obtain the coupled cluster Lagrangian,

$$\mathcal{L}_{\text{CC}} = \langle\tilde{\mathbf{C}}\mathbf{C}|\hat{H}|\mathbf{C}\mathbf{C}\rangle = \langle\mathbf{R}|(1 + \Lambda)e^{-T}\hat{H}e^T|\mathbf{R}\rangle, \quad (3)$$

where \hat{H} is the electronic Hamiltonian in the standard notation,²⁹

$$\hat{H} = \sum_{pq} h_{pq} E_{pq} + \frac{1}{2} \sum_{pqrs} g_{pqrs} (E_{pq} E_{rs} - E_{ps} \delta_{qr}). \quad (4)$$

The equations for full configuration interaction (FCI) are recovered from this Lagrangian, except for a normalization factor, if the excitation manifold is not truncated. In this case the biorthonormal left side will be equivalent to the conjugate of the right side, up to a normalization factor.

Determining the stationary points of \mathcal{L}_{CC} results in the equations for the parameters $\boldsymbol{\tau}$ and $\boldsymbol{\lambda}$. The derivatives with respect to $\boldsymbol{\lambda}$ gives the familiar coupled cluster projection equations for the amplitudes and the derivatives with respect to $\boldsymbol{\tau}$ give the equations for $\boldsymbol{\lambda}$. In practice, T and Λ are truncated at some excitation level with respect to the reference determinant.

$$T^{\text{CCSDT}} = T_1 + T_2 + T_3 \quad \Lambda^{\text{CCSDT}} = \Lambda_1 + \Lambda_2 + \Lambda_3 \quad (5)$$

The $\exp(T_1)$ operator can be viewed as a biorthogonal orbital transformation and we employ the T_1 -transformed Hamiltonian throughout,

$$H = e^{-T_1} \hat{H} e^{T_1}. \quad (6)$$

The equations for CCSDT then become those of CCDT. Inserting these definitions into \mathcal{L}_{CC} , we get the CCSDT Lagrangian,

$$\begin{aligned} \mathcal{L}_{\text{CCSDT}} = & \langle \mathbf{R} | H + [H, T_2] | \mathbf{R} \rangle \\ & + \sum_{\mu_1} \lambda_{\mu_1} \langle \mu_1 | H + [H, T_2] + [H, T_3] | \mathbf{R} \rangle \\ & + \sum_{\mu_2} \lambda_{\mu_2} \langle \mu_2 | H + [H, T_2] + \frac{1}{2} [[H, T_2], T_2] + [H, T_3] | \mathbf{R} \rangle \\ & + \sum_{\mu_3} \lambda_{\mu_3} \langle \mu_3 | [H, T_2] + \frac{1}{2} [[H, T_2], T_2] + [H, T_3] + [[H, T_2], T_3] | \mathbf{R} \rangle. \end{aligned} \quad (7)$$

The last two commutator terms of eq (7) make the full CCSDT model scale as N^8 . To reduce the cost we use a perturbation scheme,^{19,20} where the transformed Hamiltonian is divided into an effective one particle operator and a fluctuation potential, similar to MBPT,^{10,11}

$$H = F + U. \quad (8)$$

The operators are assigned orders as summarized in Table 1.

$$\begin{aligned} \mathcal{L}_{\text{CC3}} = & \sum_{\mu_1} \lambda_{\mu_1} \langle \mu_1 | H + [H, T_2] + [H, T_3] | \mathbf{R} \rangle \\ & + \sum_{\mu_2} \lambda_{\mu_2} \langle \mu_2 | H + [H, T_2] + \frac{1}{2} [[H, T_2], T_2] + [H, T_3] | \mathbf{R} \rangle \\ & + \sum_{\mu_3} \lambda_{\mu_3} \langle \mu_3 | [H, T_2] + [F, T_3] | \mathbf{R} \rangle \end{aligned} \quad (9)$$

The CC3 Lagrangian, eq (9), is obtained by discarding terms from the CCSDT Lagrangian, that are of fifth order in the perturbation and higher.

Table 1: Perturbation orders in CC3.

order	0	1	2
Hamiltonian	F	U	
Ground state	Λ_1, T_1	Λ_2, T_2	Λ_3, T_3
EOM	r, l, L_1, R_1	L_2, R_2	L_3, R_3

The singles amplitudes, both in Λ_1 and T_1 , are considered to be zeroth order in the perturbation as they are viewed as approximate orbital transformation parameters.^{30,31} However, in MBPT the first contribution of the single excitations appears in second order.

In coupled cluster theory excitation energies and other spectroscopic properties are usually computed using either CCRT or the EOM formalism. In CCRT, time dependent expectation values of molecular properties are expanded in orders of a frequency dependent perturbation. The frequency dependent expansion terms are referred to as response functions. Excitation energies and corresponding transition moments are determined from the poles and residues of the linear response function. In EOM theory, the starting point is a CI parametrization for the excited states. The eigenvalue problem for the Hamiltonian in this basis gives excited states and excitation energies. Coupled cluster response theory and EOM gives the same expressions for the excitation energies, however the transition moments differ. Although EOM transition moments are not size intensive, we expect these errors to be small for CC3.

The similarity transformed Hamiltonian is projected onto the reference and the truncated excitation manifold to obtain the Hamiltonian matrix,

$$\bar{\mathbf{H}}_{\mu\nu} = \langle \mu | e^{-T} \hat{H} e^T | \nu \rangle. \quad (10)$$

This matrix is not symmetric, hence, the left and right eigenvectors will not be Hermitian conjugates, but they will be biorthonormal.

$$\bar{\mathbf{H}} \mathbf{R}_m = E_m \mathbf{R}_m \quad \mathbf{L}_m^T \bar{\mathbf{H}} = E_m \mathbf{L}_m^T \quad \mathbf{L}_m^T \mathbf{R}_n = \delta_{m,n} \quad (11)$$

We also introduce the convenient notation

$$\mathbf{R}_m = \begin{pmatrix} r_m \\ \bar{\mathbf{R}}_m \end{pmatrix} \quad \mathbf{L}_m = \begin{pmatrix} l_m \\ \bar{\mathbf{L}}_m \end{pmatrix}, \quad (12)$$

where l_m and r_m refer to the first element of the vectors and $\bar{\mathbf{L}}_m$ and $\bar{\mathbf{R}}_m$ refer to the rest. The vectors \mathbf{L}_m and \mathbf{R}_m correspond to the operators L_m and R_m , which have a similar form to Λ and T , but also includes reference contributions. The EOM excited right states are then written as

$$|m\rangle = R_m |CC\rangle = e^T R_m |R\rangle, \quad (13)$$

and the left states are written as

$$\langle m| = \langle R| L_m e^{-T}. \quad (14)$$

Because the τ amplitudes are solutions to the coupled cluster ground state equations, the first column of $\bar{\mathbf{H}}$ is zero, except for the first element which equals the ground state energy, E_0 . The eigenvalues of $\bar{\mathbf{H}}$ correspond to the energies of the states.

$$\bar{\mathbf{H}} = \begin{pmatrix} E_0 & \boldsymbol{\eta}^T \\ \mathbf{0} & \mathbf{M} \end{pmatrix} \quad (15)$$

In the following, the index m will refer to states other than the ground state denoted by 0. From the structure of the Hamiltonian matrix, we see that the vector \mathbf{R}_0 , with the elements $r_0 = 1$ and $\bar{\mathbf{R}}_0 = \mathbf{0}$, corresponds to the ground state. For the right excited states, $\bar{\mathbf{R}}_m$ must be an eigenvector of \mathbf{M} with eigenvalue E_m . Similarly, for the left excited states $l_m = 0$ and $\bar{\mathbf{L}}_m$ has to be a left eigenvector of \mathbf{M} , due to the biorthonormality with \mathbf{R}_0 and \mathbf{R}_m . The left ground state, \mathbf{L}_0 , has the component $l_0 = 1$ and the vector $\bar{\mathbf{L}}_0$ is obtained

from the linear equation

$$\boldsymbol{\eta}^T = \bar{\mathbf{L}}_0^T (E_0 \mathbf{I} - \mathbf{M}), \quad (16)$$

where \mathbf{I} is the identity matrix. Finally, $r_m = -\bar{\mathbf{L}}_0^T \bar{\mathbf{R}}_m$ to ensure biorthogonality between \mathbf{R}_m and \mathbf{L}_0 . The matrix $\mathbf{J} = (\mathbf{M} - E_0 \mathbf{I})$ is the derivative of the Lagrangian with respect to $\boldsymbol{\tau}$ and $\boldsymbol{\lambda}$,

$$\mathbf{J}_{\mu\nu} = \frac{\partial^2 \mathcal{L}_{CC}}{\partial \lambda_\mu \partial \tau_\nu}, \quad (17)$$

and is called the Jacobian. As expected the equation for \mathbf{L}_0 is the same as for Λ . The CCSDT Jacobian is given by

$$\mathbf{J}_{CCSDT} = \begin{pmatrix} \langle \mu_1 | [H + [H, T_2], X_{\nu_1}] | \mathbf{R} \rangle & \langle \mu_1 | [H, X_{\nu_2}] | \mathbf{R} \rangle & \langle \mu_1 | [H, X_{\nu_3}] | \mathbf{R} \rangle \\ \langle \mu_2 | [H + [H, T_{2+3}], X_{\nu_1}] | \mathbf{R} \rangle & \langle \mu_2 | [H + [H, T_2], X_{\nu_2}] | \mathbf{R} \rangle & \langle \mu_2 | [H, X_{\nu_3}] | \mathbf{R} \rangle \\ \langle \mu_3 | [H + [H, T_{2+3}] + \frac{1}{2} [[H, T_2], T_2], X_{\nu_1}] | \mathbf{R} \rangle & \langle \mu_3 | [H + [H, T_{2+3}], X_{\nu_2}] | \mathbf{R} \rangle & \langle \mu_3 | [H + [H, T_2], X_{\nu_3}] | \mathbf{R} \rangle \end{pmatrix} \quad (18)$$

and the CCSDT $\boldsymbol{\eta}$ vector is given as

$$\boldsymbol{\eta}_{CCSDT}^T = \left(\langle \mathbf{R} | [H, X_{\nu_1}] | \mathbf{R} \rangle \quad \langle \mathbf{R} | [H, X_{\nu_2}] | \mathbf{R} \rangle \quad \mathbf{0}^T \right), \quad (19)$$

where T_{2+3} is shorthand notation for $T_2 + T_3$. These expressions are written in commutator form which requires that the projection equations for T are satisfied.

For EOM CC3 we introduce a perturbation expansion. Our starting point is the expression for the energy of the EOM states,

$$E_m = \mathbf{L}_m^T \bar{\mathbf{H}} \mathbf{R}_m. \quad (20)$$

We assign the same perturbation orders to \mathbf{L} and \mathbf{R} as to T and Λ , see Table 1. As CC3 does not satisfy the projection equations, the first column of $\bar{\mathbf{H}}$ will not be zero after the first element. However, the nonzero terms will be discarded as they are at least fifth order in the perturbation. In order to derive the correct CC3 Jacobian, known from CCRT, we discard

terms from the CCSDT Jacobian in commutator form using perturbation theory, giving

$$\mathbf{J}_{CC3} = \begin{pmatrix} \langle \mu_1 | [H + [H, T_2], X_{\nu_1}] | \mathbf{R} \rangle & \langle \mu_1 | [H, X_{\nu_2}] | \mathbf{R} \rangle & \langle \mu_1 | [H, X_{\nu_3}] | \mathbf{R} \rangle \\ \langle \mu_2 | [H + [H, T_{2+3}], X_{\nu_1}] | \mathbf{R} \rangle & \langle \mu_2 | [H + [H, T_2], X_{\nu_2}] | \mathbf{R} \rangle & \langle \mu_2 | [H, X_{\nu_3}] | \mathbf{R} \rangle \\ \langle \mu_3 | [H + [H, T_2], X_{\nu_1}] | \mathbf{R} \rangle & \langle \mu_3 | [H, X_{\nu_2}] | \mathbf{R} \rangle & \langle \mu_3 | [F, X_{\nu_3}] | \mathbf{R} \rangle \end{pmatrix}. \quad (21)$$

To obtain EOM transition moments, the biorthogonal states are inserted into the expressions for the CI transition moments. For a given one-electron operator, $A = \sum_{pq} A_{pq} X_{pq}$, the transition moments are expressed in terms of left and right transition density matrices,^{32,33} $\tilde{\mathbf{D}}^{n,m}$ and $\mathbf{D}^{n,m}$:

$$\langle \tilde{\mathbf{C}}\mathbf{C} | A | \mathbf{m} \rangle \langle \mathbf{m} | A | \mathbf{C}\mathbf{C} \rangle = \sum_{pq} (\tilde{D}_{pq}^{0,m} A_{pq}) \times \sum_{pq} (D_{pq}^{m,0} A_{pq}). \quad (22)$$

The elements of the right transition density are defined as:

$$D_{pq}^{m,0} = \langle \mathbf{m} | X_{pq} | \mathbf{C}\mathbf{C} \rangle, \quad (23)$$

while the elements of $\tilde{\mathbf{D}}^{0,m}$ are given by

$$\begin{aligned} \tilde{D}_{pq}^{0,m} &= \langle \tilde{\mathbf{C}}\mathbf{C} | X_{pq} | \mathbf{m} \rangle \\ &= \langle \mathbf{R} | (1 + \Lambda) e^{-T} X_{pq} e^T R_m | \mathbf{R} \rangle \\ &= \langle \mathbf{R} | (1 + \Lambda) e^{-T} X_{pq} e^T \bar{R}_m | \mathbf{R} \rangle \\ &\quad + r_m \langle \mathbf{R} | (1 + \Lambda) e^{-T} X_{pq} e^T | \mathbf{R} \rangle \\ &= \bar{D}_{pq}^{0,m} - r_m D_{pq}^{0,0}, \end{aligned} \quad (24)$$

where $\mathbf{D}^{0,0}$ is the ground state density.

Implementation

The closed shell CC3 ground state, singlet excitation energies, and EOM transition moments have been implemented in the e^T program.³⁴ In the following we use the standard notation, the indices $i, j, k \dots$ refer to occupied, $a, b, c \dots$ to virtual and $p, q, r \dots$ to general orbitals. The core part of the algorithms is a triple loop over the occupied indices $i \geq j \geq k$ as proposed for CCSD(T) by Rendell *et al.*³⁵ and for CC3 by Myhre and Koch.²⁰ An outline of the algorithm to construct the ground state equations is given in Algorithm 1. Within the triple loop we first construct the triples amplitudes for a given set of $\{i, j, k\}$ and contract those amplitudes with integrals to obtain the triples contribution to the ground state residual vector, $\mathbf{\Omega}$. Only n_V^3 amplitudes are stored in memory at any time. The computational cost of constructing the triples amplitudes is reduced by a factor of six by restricting the loop indices and exploiting the permutational symmetry,

$$\tau_{ijk}^{abc} = \tau_{jik}^{bac} = \tau_{kji}^{cba} = \tau_{ikj}^{acb} = \tau_{kij}^{cab} = \tau_{jki}^{bca}. \quad (25)$$

In order to avoid reading two-electron integrals from file inside the loop, the program checks if all the integrals can be kept in memory, otherwise they are read in batches of i, j, k in additional outer loops. To minimize reordering inside the loop and ensure efficient matrix contractions, the integrals are reordered and written to disk before entering the loop. To make use of the permutational symmetry of the amplitudes, they are reordered inside the loop over the occupied orbitals and the reordering scales as $n_V^3 n_O^3$. These operations are parallelized using OpenMP, but they are memory bound and may parallelize poorly.³⁶

The algorithm to construct the triples contribution to the ground state residual, $\mathbf{\Omega}$, is outlined in Algorithm 1. Integrals in T_1 -transformed basis are denoted by g_{pqrs} and the intermediate

$$\gamma_{pqrs} = 2g_{pqrs} - g_{psrq} = 2g_{pqrs} - g_{rqp} \quad (26)$$

is constructed from these integrals. The equation for the triples amplitudes includes a

permutation operator, defined by

$$P_{ijk}^{abc} B_{ijk}^{abc} = B_{ijk}^{abc} + B_{jik}^{bac} + B_{kji}^{cba} + B_{ikj}^{acb} + B_{jki}^{bca} + B_{kij}^{cab}. \quad (27)$$

To recover all contributions to the Ω vector from the restricted loops, all unique permutations of i, j, k have to be considered. This results in six terms when all the occupied indices are unique and three terms in the case of two occupied indices being equal. If all three occupied indices are identical, there is no contribution, as this corresponds to a triple excitation from a single orbital.

Algorithm 1 Algorithm to construct the CC3 ground state equations.

```

while not converged do
  for  $i = 1, n_O$  do
    for  $j = 1, i$  do
      for  $k = 1, j$  do
         $\tau_{ijk}^{abc} = -(\varepsilon_{ijk}^{abc})^{-1} P_{ijk}^{abc} \left( \sum_d \tau_{ij}^{ad} g_{bdck} - \sum_l \tau_{il}^{ab} g_{ljck} \right)$ 

        for Permutations of  $i, j, k$  do
           $\Omega_i^a += \sum_{jk}^{bc} (\tau_{ijk}^{abc} - \tau_{ijk}^{cba}) \gamma_{jbbkc}$ 
           $\Omega_{ij}^{ab} += P_{ij}^{ab} \sum_k^c (\tau_{ijk}^{abc} - \tau_{ijk}^{cba}) F_{kc}$ 
           $\Omega_{il}^{ab} -= P_{il}^{ab} \sum_{jk}^c (2\tau_{ijk}^{abc} - \tau_{ijk}^{acb} - \tau_{ijk}^{cba}) g_{jllkc}$ 
           $\Omega_{ij}^{ad} += P_{ij}^{ad} \sum_k^{bc} (2\tau_{ijk}^{abc} - \tau_{ijk}^{acb} - \tau_{ijk}^{cba}) g_{dbkc}$ 
        end for
      end for
    end for
  end while

```

For excited state calculations, we may reduce the iterative cost from $5n_{\nabla}^4 n_O^3$ to $4n_{\nabla}^4 n_O^3$ by constructing τ_3 -dependent intermediates. This is carried out in a preparation routine outlined in Algorithm 2. The same intermediates are used in the algorithms for both \mathbf{L} and \mathbf{R} . Nevertheless, we still have to construct the τ_3 amplitudes in each iteration, see supporting information. It would be possible to construct an intermediate of size $n_{\nabla}^3 n_O^3$ for this term as well, reducing the iterative computational scaling to $3n_{\nabla}^4 n_O^3$, however, constructing this

intermediate scales as $n_V^4 n_O^4$.

Algorithm 2 Preparation for the CC3 Jacobian transformations.

```

for  $i = 1, n_O$  do
  for  $j = 1, i$  do
    for  $k = 1, j$  do
       $\tau_{ijk}^{abc} = -(\varepsilon_{ijk}^{abc})^{-1} P_{ijk}^{abc} \left( \sum_d \tau_{ij}^{ad} g_{bdck} - \sum_l \tau_{il}^{ab} g_{ljck} \right)$ 
      for Permutations of  $i, j, k$  do
         $Z_{abid} = -\sum_{jk}^c (2\tau_{ijk}^{abc} - \tau_{ijk}^{acb} - \tau_{ijk}^{cba}) g_{jdkc}$ 
         $Z_{ajil} = -\sum_{bc}^k (2\tau_{ijk}^{abc} - \tau_{ijk}^{acb} - \tau_{ijk}^{cba}) g_{lbkc}$ 
      end for
    end for
  end for
end for

```

The algorithm for the Jacobian transformation of a trial vector, see supporting information, resembles the algorithm for the ground state, but it is separated into two loops. In the first, $\boldsymbol{\tau}_3$ is constructed and contracted with an \mathbf{R}_1 -dependent intermediate. In the second loop, the routine used to construct $\boldsymbol{\tau}_3$ is used again, but called twice with different input tensors to construct \mathbf{R}_3 . The excitation vector is then contracted with the same integrals as the ground state to construct the excited state residual vector.

The algorithm for the transpose Jacobian transformation, is similar to the right transformation. First, the $\boldsymbol{\tau}_3$ amplitudes are constructed and contracted in a separate loop over i, j, k , before the main loop, where the \mathbf{L}_3 amplitudes are constructed. However, the left side is more complicated, involving outer products and several intermediates. The construction of \mathbf{L}_3 , see supporting information, includes two matrix products scaling as $n_V^4 n_O^3$, but these can be combined into a single matrix product due to the permutation operator. A complication for the transpose transformation is that it requires construction of intermediates inside the i, j, k loop. One of these intermediates requires $n_V^3 n_O$ memory and we have to add batching functionality, writing and reading the intermediate from file for each batch. Overall, the scaling is $4n_V^4 n_O^3$, the same as for the right transformation.

In Algorithm 3 we show how to compute the \mathbf{L}_3 contributions to $\mathbf{D}^{m,0}$, see eq (23). The

Algorithm 3 Algorithm to compute the CC3 contribution to $D^{m,0}$.

```

for i = 1,  $n_O$  do
  for j = 1, i do
    for k = 1, j do
       $\tau_{ijk}^{abc} = -(\varepsilon_{ijk}^{abc})^{-1} P_{ijk}^{abc} \left( \sum_d \tau_{ij}^{ad} g_{bdck} - \sum_l \tau_{il}^{ab} g_{ljck} \right)$ 
       $L_{ijk}^{abc} = (\omega - \varepsilon_{ijk}^{abc})^{-1} P_{ijk}^{abc} \left( L_i^a \gamma_{jbkc} - L_k^a \gamma_{jbic} + L_{ij}^{ab} F_{kc} - L_{ik}^{ab} F_{jc} \right.$ 
         $\quad + \sum_l (L_{lk}^{ab} g_{iljc} - L_{il}^{ab} \gamma_{jlkc})$ 
         $\quad \left. - \sum_d (L_{jk}^{ad} g_{ibdc} - L_{ij}^{ad} \gamma_{dbkc}) \right)$ 

      for Permutations of  $i, j, k$  do
         $D_{kc}^{m,0} \leftarrow \sum_{ij}^{ab} (\tau_{ijk}^{abc} - \tau_{ijk}^{acb}) L_{ij}^{ab}$ 
         $Y_{clik} = \sum_j^{ab} L_{ijk}^{abc} \tau_{lj}^{ab}$ 
         $D_{cd}^{m,0} \leftarrow \frac{1}{2} \sum_{ijk}^{ab} L_{ijk}^{abc} \tau_{ijk}^{abd}$ 
      end for

    end for
  end for
end for

 $D_{ld}^{m,0} \leftarrow - \sum_{ik}^c Y_{clik} \tau_{ki}^{cd}$ 

for a = 1,  $n_V$  do
  for b = 1, a do
    for c = 1, b do
       $\tau_{ijk}^{abc} = -(\varepsilon_{ijk}^{abc})^{-1} P_{ijk}^{abc} \left( \sum_d \tau_{ij}^{ad} g_{bdck} - \sum_l \tau_{il}^{ab} g_{ljck} \right)$ 
       $L_{ijk}^{abc} = (\omega - \varepsilon_{ijk}^{abc})^{-1} P_{ijk}^{abc} \left( L_i^a \gamma_{jbkc} - L_k^a \gamma_{jbic} + L_{ij}^{ab} F_{kc} - L_{ik}^{ab} F_{jc} \right.$ 
         $\quad + \sum_l (L_{lk}^{ab} g_{iljc} - L_{il}^{ab} \gamma_{jlkc})$ 
         $\quad \left. - \sum_d (L_{jk}^{ad} g_{ibdc} - L_{ij}^{ad} \gamma_{dbkc}) \right)$ 

      for Permutations of  $a, b, c$  do
         $D_{lk}^{m,0} \leftarrow -\frac{1}{2} \sum_{ij}^{abc} L_{ijk}^{abc} \tau_{ijl}^{abc}$ 
      end for

    end for
  end for
end for

```

same algorithm can be used to compute the ground state density, $\mathbf{D}^{0,0}$, by inserting $\mathbf{\Lambda}_3$ instead of \mathbf{L}_3 . For $\tilde{\mathbf{D}}^{0,m}$ several intermediates from the ground state density, as well as the ground state density itself, are reused, see the supporting information.

The main difference between Algorithm 3 and the algorithm for the Jacobian transformations is the additional triple loop over the virtual indices. This loop is required due to the occupied-occupied block of the density matrix that has contributions from two triples tensors with different occupied indices. Therefore, it is not possible to use the previous scheme of holding only triples amplitudes for a given i, j, k . In systems usually treated with CC3 the number of occupied orbitals is small compared with the number of virtual orbitals, when a reasonable basis set is used. Therefore, the BLAS³⁷ routines do not parallelize well, and the serial loop over the virtual indices would constitute the bottleneck of the calculation. To circumvent that, the loops over the virtual indices were parallelized using OpenMP.³⁶

The triples tensors have to be constructed once for fixed occupied and once for fixed virtual indices and the computational cost of constructing the CC3 transition densities increases to $13n_V^4 n_O^3$ per state. Nevertheless, when considering timings the construction of the densities constitutes only a small fraction of the time compared to the iterative solution of the excited state equations.

Applications

To demonstrate the performance of the code, we have calculated singlet valence and core excitation energies and EOM oscillator strengths for the amino acid L-proline ($\text{C}_5\text{H}_9\text{NO}_2$).³⁸ One valence excitation energy was calculated at the CCSD/aug-cc-pVTZ and CC3/aug-cc-pVTZ levels of theory using the frozen core (FC) approximation resulting in 23 occupied and 544 virtual orbitals. Table 2 shows the excitation energy and oscillator strength for the lowest valence excited state at the CCSD and CC3 level. The excitation vector has 96% singles contribution and the excitation energies differ by about 0.11 eV. In Table 3, we report

the averaged time per routine call as well as the number of routine calls. For the ground state n_{calls} specifies the number of times the ground state residual vector is computed. For the right and left excited states the number of calls to the Jacobian transformations are reported.

Table 2: Proline excitation energy and oscillator strength for the lowest singlet valence excitation at the CCSD and CC3 levels of theory. Note that the oscillator strengths f are scaled by a factor of 100.

CCSD		CC3	
ω [eV]	f	ω [eV]	f
5.830	0.0775	5.718	0.0661

Table 3: Timings for the different parts of the calculation of one valence excited state with oscillator strengths in L-proline at the CC3 level of theory. n_{calls} specifies the number of calls to the subroutines constructing the respective quantity. Timings have been averaged over the number of routine calls. The calculations were performed on one node with two Intel Xeon Gold 6152 processors with 22 cores each and using a total of 700 GB shared memory.

Contributions	walltime [min]	n_{calls}
Ground state	163	10
Prepare for multipliers	169	1
Multipliers	347	11
Prepare for Jacobian	147	1
Right excited states	281	26
Prepare for Jacobian	160	1
Left excited states	341	28
$\mathbf{D}^{0,0}$	379	1
$\mathbf{D}^{m,0}$	382	1
$\tilde{\mathbf{D}}^{0,m}$	530	1

From Table 3 we observe that one iteration of the multiplier equations is approximately twice as expensive as one iteration for the ground state. The transpose Jacobian transformation, which is required for the multipliers, scales as $4n_{\text{v}}^4 n_{\text{O}}^3$ compared to a scaling of $2n_{\text{v}}^4 n_{\text{O}}^3$ for the ground state. The timings to obtain left excited states are roughly the same as the timings to solve for the multipliers because a trial vector is transformed by the transpose of the Jacobian. In the preparation routines the intermediates used in the Jacobian trans-

formations are computed, as shown in Algorithm 2. The preparation is as expensive as one iteration for the ground state, but we save one $n_V^4 n_O^3$ contraction per Jacobian transformation. The ground state density and $\mathbf{D}^{m,0}$ are calculated using the same routines and the computational cost is the same. The CC3 contribution to $\tilde{\mathbf{D}}^{0,m}$ requires $\boldsymbol{\tau}_3$, $\boldsymbol{\lambda}_3$ and \mathbf{R}_3 . In addition, \mathbf{R}_3 is approximately twice as expensive to compute as $\boldsymbol{\tau}_3$, so $\tilde{\mathbf{D}}^{0,m}$ is considerably more expensive than $\mathbf{D}^{m,0}$.

We have also calculated six core excited states for each of the oxygen atoms, using core valence separation (CVS). The aug-cc-pCVTZ basis set is used on the oxygen atom that was excited and aug-cc-pVDZ for the rest of the molecule (31 occupied and 270 virtual orbitals). In Table 4 we show the results for core excitations from the carbonyl oxygen of L-proline. Due to the better description of relaxation effects by the inclusion of triple excitations, the excitation energies obtained with CC3 are up to 3 eV lower than the corresponding CCSD excitation energies. The same trends are observed for core excitations from the hydroxyl oxygen, as shown in Table 5. The CC3 oscillator strengths are between 16% and 60% lower than the values obtained with CCSD. In Figure 1 we show NEXAFS spectra computed with EOM-CCSD and EOM-CC3. Despite shifting the CCSD spectrum by -1.9 eV, the two spectra show significant differences. From the CCSD spectrum one would expect two peaks between 535 eV and 536 eV if the resolution is high enough. Additionally, the peak at 534 eV is not present in the shifted CCSD plot, where the corresponding state is shifted by more than 1.3 eV. The calculated CC3 excitation energies are in good agreement with experimental data reported by Plekan *et al.* in Ref. 39. The authors measured the first excitation from the carbonyl oxygen at 532.2 eV and a broad peak from the hydroxyl oxygen at 535.4 eV, consistent with the first two calculated CC3 excitation energies. Note that taking relativistic effects into account will increase the excitation energies by about 0.38 eV, while increasing the basis set would lower them somewhat.^{9,40}

Timings for the calculations of the core excited states are reported in Table 6 for excitations from the hydroxyl oxygen. The timings for the core excitations from the carbonyl

Table 4: Proline excitation energies (in eV) and oscillator strengths for core excitations from the carbonyl oxygen at the CCSD and CC3 level of theory. Note that the oscillator strengths f are scaled by a factor of 100.

CCSD		CC3	
ω	f	ω	f
533.943	3.6218	532.040	2.8536
537.103	0.1238	533.818	0.0953
538.104	0.2566	534.757	0.1377
538.335	0.1477	534.954	0.0988
538.710	0.1779	535.180	0.0261
539.207	0.0761	535.677	0.0340

Table 5: Proline excitation energies (in eV) and oscillator strengths for core excitations from the hydroxyl oxygen at the CCSD and CC3 level of theory. Note that the oscillator strengths f are scaled by a factor of 100.

CCSD		CC3	
ω	f	ω	f
537.172	1.6373	535.093	0.9192
537.911	1.3923	535.186	0.9350
539.598	0.6640	536.789	0.2758
539.770	0.4145	536.955	0.2643
540.165	0.3164	537.235	0.1824
540.736	0.3508	537.747	0.2088

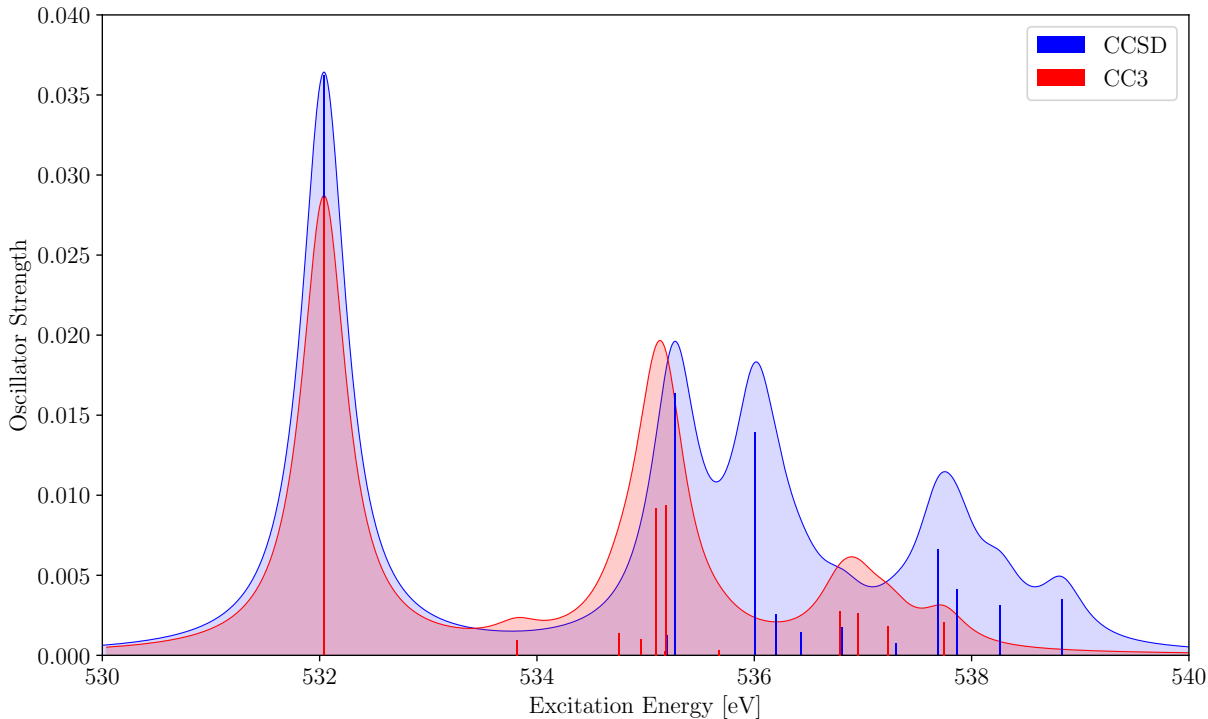


Figure 1: Core excitation spectrum of the oxygen edge of L-proline computed with CC3 (red) and CCSD (blue). The peaks were broadened using a Lorentzian lineshape and a width of 0.5 eV. The CCSD spectrum is shifted by -1.9 eV to match the oxygen edge of the CC3 spectrum.

oxygen are not reported because they are almost identical. Compared to the valence excited state calculation the timings for the ground state and the multipliers are reduced due to the use of smaller basis sets. The CVS approximation reduces the computational cost of the Jacobian transformations from $4n_V^4 n_O^3$ to $4n_V^4 n_O^2$. Therefore, one iteration is 4 to 5 times faster compared to one iteration of the ground state. These savings are achieved by cycling the triple loop over the occupied indices when none of the indices correspond to the core orbitals of interest. Similar savings can be achieved during the construction of the transition densities. However, in the present implementation only the triple loop over the occupied indices can be cycled but not the loops over the virtual indices.

In Table 7, we present timings from calculations on furan, using 1, 5, 10, 20 and 40 threads. We calculated the transition moments from the ground state to the first excited

Table 6: Timings for the different parts of the calculation of 4 core excited states (located at the hydroxyl oxygen) with oscillator strengths for L-proline at the CC3 level of theory. n_{calls} specifies the number of calls to the subroutines constructing the respective quantities. Timings have been averaged over the number of routine calls. The calculations were performed on nodes with two Intel Xeon Gold 6152 processors with 22 cores each and using a total of 700 GB shared memory.

Contributions	walltime [min]	n_{calls}
Ground state	22	14
Prepare for multipliers	18	1
Multipliers	49	11
Prepare for Jacobian	18	2
Right excited states	4	229
Left excited states	5	285
$\mathbf{D}^{0,0}$	65	1
$\mathbf{D}^{m,0}$	22	4
$\tilde{\mathbf{D}}^{0,m}$	63	4

state, which requires solving for $\boldsymbol{\tau}$, $\boldsymbol{\lambda}$, \mathbf{R} and \mathbf{L} . We also report speedups relative to the single thread calculation. While the speedup is not perfect, increasing the number of threads from 1 to 40 reduces the total wall time by more than an order of magnitude. Note that these calculations were performed with a newer version of e^T than the proline calculations above.

Table 7: Timings for calculating the EOM transition moment for the first excited state of furan using 1, 5, 10, 20 and 40 threads. Total times as well as timings for solving for the $\boldsymbol{\tau}$, $\boldsymbol{\lambda}$, \mathbf{R} and \mathbf{L} are reported. Numbers of iterations are given in parentheses, The speedup compared to the row above is given next to the timing. The remaining time is primarily spent constructing the density matrices. The calculations were performed on nodes with two Intel Xeon Gold 6138 processors with 20 cores each and using a total of 150 GB shared memory.

Threads	total		$\boldsymbol{\tau}$ (9)		$\boldsymbol{\lambda}$ (10)		\mathbf{R} (14)		\mathbf{L} (17)	
1	29783	-	3237	-	5983	-	7709	-	9672	-
5	8365	3.56	805	4.02	1711	3.50	2225	3.46	2833	3.41
10	4971	5.99	521	6.21	1067	5.61	1432	5.38	1491	6.49
20	3811	7.82	418	7.74	590	10.14	1192	6.47	1291	7.49
40	2625	11.35	313	10.34	554	10.80	673	11.45	851	11.37

Finally, in Figure 2, we show the CC3 transition density, $\tilde{\mathbf{D}}_{CC3}^{0,2}$, as well as the difference

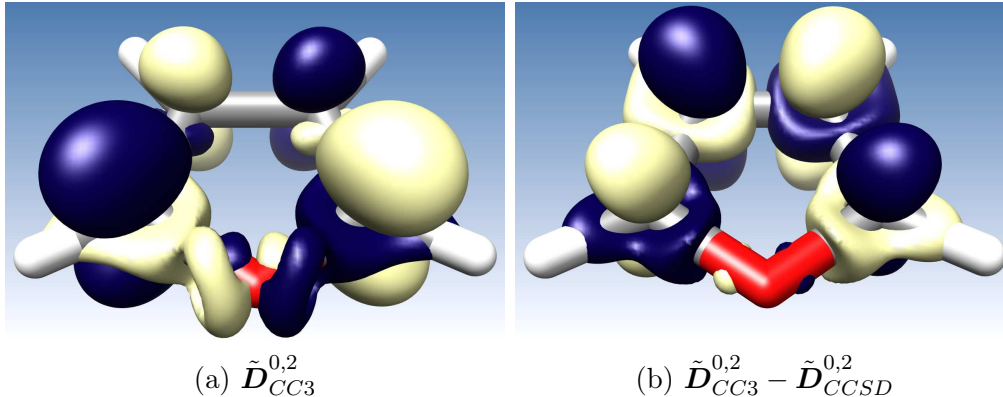


Figure 2: Transition densities of furan. (a) The second CC3 transition density ($\tilde{\mathbf{D}}^{CC3}$) with contour value 0.006. (b) Difference from CCSD ($\tilde{\mathbf{D}}_{CC3}^{0,2} - \tilde{\mathbf{D}}_{CCSD}^{0,2}$) with contour value 0.0003.

between the CC3 and CCSD transition densities, $\tilde{\mathbf{D}}_{CC3}^{0,2} - \tilde{\mathbf{D}}_{CCSD}^{0,2}$, plotted using Chimera.⁴¹ While the difference between the densities is small (the contour value is only 0.0003), the triples decrease the magnitude of the transition density. This is reflected in a reduction of the oscillator strength from 0.181 to 0.168, and appears to be a general trend when going from CCSD to CC3.

Conclusion

In this paper we have described an efficient implementation of the CC3 model including ground state and excited state energies as well as EOM oscillator strengths. To the best of our knowledge, the algorithm reported is the most efficient for CC3 and the first implementation of EOM-CC3. Due to the use of the permutational symmetry of the triples amplitudes, the computational cost of computing the triples part of the amplitudes is reduced by a factor of 6. The code is parallelized using OpenMP and the algorithm can be extended to utilize MPI through coarrays which are included in the Fortran 2008 standard.

The transition density algorithm is currently not optimal and we intend to explore calculating the contributions in a single triple loop over the virtual orbitals. This would require storage of a subset of amplitudes scaling as $n_{\vee}n_{\text{O}}^3$ in memory. Parallelization will then happen in the triple loop. It is possible that such a parallelization scheme, would be more

efficient for all algorithms presented in this paper and we intend to explore this further. An immediate optimization is to directly contract the intermediates in the Jacobian transpose algorithm with Cholesky vectors, avoiding construction of the n_V^4 integrals.

Finally, the extension to the densities of excited states and the transition densities between excited states is straightforward and will be reported elsewhere.

Acknowledgement

We acknowledge computing resources through UNINETT Sigma2 - the National Infrastructure for High Performance Computing and Data Storage in Norway, through project number NN2962k. We acknowledge funding from the Marie Skłodowska-Curie European Training Network “COSINE – COmputational Spectroscopy In Natural sciences and Engineering”, Grant Agreement No. 765739 and the Research Council of Norway through FRINATEK projects 263110, CCGPU, and 275506, TheoLight.

References

- (1) Holch, F.; Hübner, D.; Fink, R.; Schöll, A.; Umbach, E. New set-up for high-quality soft-X-ray absorption spectroscopy of large organic molecules in the gas phase. *J. Electron Spectrosc. Relat. Phenom.* **2011**, *184*, 452 – 456.
- (2) Scholz, M.; Holch, F.; Sauer, C.; Wiessner, M.; Schöll, A.; Reinert, F. Core Hole-Electron Correlation in Coherently Coupled Molecules. *Phys. Rev. Lett.* **2013**, *111*, 048102.
- (3) Norman, P.; Dreuw, A. Simulating X-ray Spectroscopies and Calculating Core-Excited States of Molecules. *Chem. Rev.* **2018**, *118*, 7208–7248.
- (4) Myhre, R. H.; Wolf, T. J. A.; Cheng, L.; Nandi, S.; Coriani, S.; Gühr, M.; Koch, H. A theoretical and experimental benchmark study of core-excited states in nitrogen. *J. Chem. Phys.* **2018**, *148*, 064106.
- (5) Liu, J.; Matthews, D.; Coriani, S.; Cheng, L. Benchmark Calculations of K-Edge Ionization Energies for First-Row Elements Using Scalar-Relativistic Core-Valence-Separated Equation-of-Motion Coupled-Cluster Methods. *J. Chem. Theory Comput.* **2019**, *15*, 1642–1651.
- (6) Helgaker, T.; Coriani, S.; Jørgensen, P.; Kristensen, K.; Olsen, J.; Ruud, K. Recent Advances in Wave Function-Based Methods of Molecular-Property Calculations. *Chem. Rev.* **2012**, *112*, 543–631.
- (7) Koch, H.; Jørgensen, P. Coupled cluster response functions. *J. Chem. Phys.* **1990**, *93*, 3333–3344.
- (8) Pedersen, T. B.; Koch, H. Coupled cluster response functions revisited. *J. Chem. Phys.* **1997**, *106*, 8059–8072.

- (9) Myhre, R. H.; Coriani, S.; Koch, H. X-ray and UV Spectra of Glycine within Coupled Cluster Linear Response Theory. *J. Phys. Chem. A* **2019**, *123*, 9701–9711.
- (10) Møller, C.; Plesset, M. S. Note on an Approximation Treatment for Many-Electron Systems. *Phys. Rev.* **1934**, *46*, 618–622.
- (11) Brueckner, K. A. Two-Body Forces and Nuclear Saturation. III. Details of the Structure of the Nucleus. *Phys. Rev.* **1955**, *97*, 1353–1366.
- (12) Barlett, R. J.; Sekino, H.; Purvis III, G. D. Comparison of MBPT and coupled-cluster methods with full CI. Importance of triplet excitation and infinite summations. *Chem. Phys. Lett.* **1983**, *98*, 66 – 71.
- (13) Urban, M.; Noga, J.; Cole, S. J.; Bartlett, R. J. Towards a full CCSDT model for electron correlation. *J. Chem. Phys.* **1985**, *83*, 4041–4046.
- (14) Raghavachari, K.; Trucks, G. W.; Pople, J. A.; Head-Gordon, M. A fifth-order perturbation comparison of electron correlation theories. *Chem. Phys. Lett.* **1989**, *157*, 479 – 483.
- (15) Stanton, J. F. Why CCSD(T) works: a different perspective. *Chem. Phys. Lett.* **1997**, *281*, 130 – 134.
- (16) Taube, A. G.; Bartlett, R. J. Improving upon CCSD(T): Λ CCSD(T). I. Potential energy surfaces. *J. Chem. Phys.* **2008**, *128*, 044110.
- (17) Matthews, D. A.; Stanton, J. F. A new approach to approximate equation-of-motion coupled cluster with triple excitations. *J. Chem. Phys.* **2016**, *145*, 124102.
- (18) Noga, J.; Bartlett, R. J.; Urban, M. Towards a full CCSDT model for electron correlation. CCSDT-n models. *Chem. Phys. Lett.* **1987**, *134*, 126 – 132.

- (19) Koch, H.; Christiansen, O.; Jørgensen, P.; Sánchez de Merás, A. M.; Helgaker, T. The CC3 model: An iterative coupled cluster approach including connected triples. *J. Chem. Phys.* **1997**, *106*, 1808–1818.
- (20) Myhre, R. H.; Koch, H. The multilevel CC3 coupled cluster model. *J. Chem. Phys.* **2016**, *145*.
- (21) Koch, H.; Christiansen, O.; Jørgensen, P.; Olsen, J. Excitation energies of BH, CH₂ and Ne in full configuration interaction and the hierarchy CCS, CC2, CCSD and CC3 of coupled cluster models. *Chemical Physics Lett.* **1995**, *244*, 75 – 82.
- (22) Kállay, M.; Gauss, J. Approximate treatment of higher excitations in coupled-cluster theory. II. Extension to general single-determinant reference functions and improved approaches for the canonical Hartree-Fock case. *The Journal of Chemical Physics* **2008**, *129*, 144101.
- (23) Stanton, J. F.; Bartlett, R. J. The equation of motion coupled-cluster method. A systematic biorthogonal approach to molecular excitation energies, transition probabilities, and excited state properties. *J. Chem. Phys.* **1993**, *98*, 7029–7039.
- (24) Koch, H.; Kobayashi, R.; Sánchez de Merás, A.; Jørgensen, P. Calculation of size-intensive transition moments from the coupled cluster singles and doubles linear response function. *J. Chem. Phys.* **1994**, *100*, 4393–4400.
- (25) Hald, K.; Jørgensen, P.; Christiansen, O.; Koch, H. Implementation of electronic ground states and singlet and triplet excitation energies in coupled cluster theory with approximate triples corrections. *J. Chem. Phys.* **2002**, *116*, 5963–5970.
- (26) Cederbaum, L. S.; Domcke, W.; Schirmer, J. Many-body theory of core holes. *Phys. Rev. A* **1980**, *22*, 206–222.

- (27) Coriani, S.; Koch, H. Communication: X-ray absorption spectra and core-ionization potentials within a core-valence separated coupled cluster framework. *J. Chem. Phys.* **2015**, *143*, 181103.
- (28) Coriani, S.; Koch, H. Erratum: “Communication: X-ray absorption spectra and core-ionization potentials within a core-valence separated coupled cluster framework” *J. Chem. Phys.* **2016**, *145*, 149901.
- (29) Helgaker, T.; Jørgensen, P.; Olsen, J. *Molecular Electronic-Structure Theory*; John Wiley & Sons, LTD: The Atrium, Southern Gate, Chichester, West Sussex, PO19 8SQ, England, 2004.
- (30) Pedersen, T. B.; Fernández, B.; Koch, H. Gauge invariant coupled cluster response theory using optimized nonorthogonal orbitals. *J. Chem. Phys.* **2001**, *114*, 6983–6993.
- (31) Kvaal, S. Ab initio quantum dynamics using coupled-cluster. *J. Chem. Phys.* **2012**, *136*, 194109.
- (32) Stanton, J. F. Separability properties of reduced and effective density matrices in the equation-of-motion coupled cluster method. *J. Chem. Phys.* **1994**, *101*, 8928–8937.
- (33) Levchenko, S. V.; Wang, T.; Krylov, A. I. Analytic gradients for the spin-conserving and spin-flipping equation-of-motion coupled-cluster models with single and double substitutions. *J. Chem. Phys.* **2005**, *122*, 224106.
- (34) Folkestad, S. D. et al. eT 1.0: An open source electronic structure program with emphasis on coupled cluster and multilevel methods. *J. Chem. Phys.* **2020**, *152*, 184103.
- (35) Rendell, A. P.; Lee, T. J.; Komornicki, A. A parallel vectorized implementation of triple excitations in CCSD(T): application to the binding energies of the AlH_3 , AlH_2F , AlHF_2 and AlF_3 dimers. *Chem. Phys. Lett.* **1991**, *178*, 462 – 470.

- (36) OpenMP Architecture Review Board, OpenMP Application Program Interface Version 5.0. 2018; <https://www.openmp.org/wp-content/uploads/OpenMP-API-Specification-5.0.pdf>.
- (37) Lawson, C. L.; Hanson, R. J.; Kincaid, D. R.; Krogh, F. T. Basic Linear Algebra Subprograms for Fortran Usage. *ACM Trans. Math. Softw.* **1979**, *5*, 308–323.
- (38) National Center for Biotechnology Information, PubChem Database. L-Proline. 2020; <https://pubchem.ncbi.nlm.nih.gov/compound/L-Proline>, CID=145742.
- (39) Plekan, O.; Feyer, V.; Richter, R.; Coreno, M.; de Simone, M.; Prince, K.; Caravetta, V. An X-ray absorption study of glycine, methionine and proline. *J. Electron Spectrosc. Relat. Phenom.* **2007**, *155*, 47 – 53.
- (40) Carbone, J. P.; Cheng, L.; Myhre, R. H.; Matthews, D.; Koch, H.; Coriani, S. An analysis of the performance of core-valence separated coupled cluster methods for core excitations and core ionizations using standard basis sets. *Adv. Quantum Chem.* **2019**,
- (41) Pettersen, E. F.; Goddard, T. D.; Huang, C. C.; Couch, G. S.; Greenblatt, D. M.; Meng, E. C.; Ferrin, T. E. UCSF Chimera – a visualization system for exploratory research and analysis. *J. Comput. Chem.* **2004**, *25*, 1605 – 1612, <https://www.cgl.ucsf.edu/chimera/>.

Graphical TOC Entry

